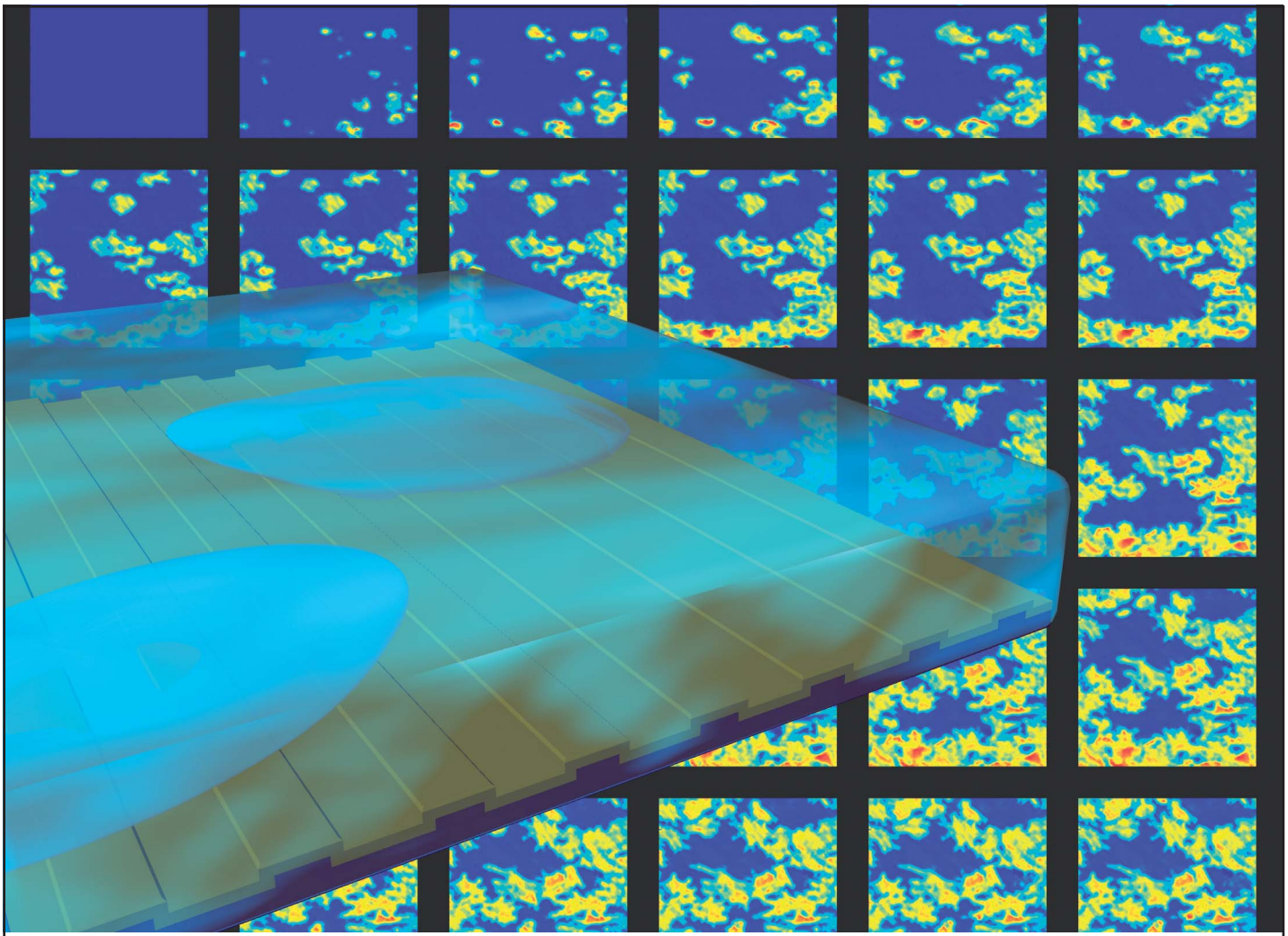

Showcasing Photonic Crystal Enhanced Microscopy: A new label-free imaging method for quantitative imaging of live cell adhesion, representing one of the optics-based biosensor technologies developed by the Nano Sensors Group at the University of Illinois at Urbana-Champaign, directed by Professor Brian T. Cunningham. More information can be found at: nano.ece.illinois.edu.

Title: Photonic crystal enhanced microscopy for imaging of live cell adhesion

Photonic Crystal Enhanced Microscopy is a new label-free cell imaging technique quantifying cell-surface interactions with high spatial resolution for observation of intracellular gradients in cell adhesion strength that occur during adhesion, chemotaxis, metastasis and apoptosis.

As featured in:

See Cunningham *et al.*, *Analyst*, 2013, **138**, 5886.

RSC Publishing

www.rsc.org/analyst

Registered Charity Number 207890

Analyst

RSC Publishing

PAPER

View Article Online
View Journal | View Issue

Cite this: *Analyst*, 2013, **138**, 5886

Photonic crystal enhanced microscopy for imaging of live cell adhesion†

Weili Chen,‡[a] Kenneth D. Long,‡[b] Meng Lu,‡[a] Vikram Chaudhery,[a] Hojeong Yu,[a] Ji Sun Choi,[c] James Polans,[a] Yue Zhuo,[b] Brendan A. C. Harley[cd] and Brian T. Cunningham*[ab]

A form of microscopy that utilizes a photonic crystal biosensor surface as a substrate for cell attachment enables label-free, quantitative, submicron resolution, time-resolved imaging of cell–surface interactions without cytotoxic staining agents or temporally-unstable fluorophores. Other forms of microscopy do not provide this direct measurement of live cell–surface attachment localization and strength that includes unique, dynamic morphological signatures critical to the investigation of important biological phenomena such as stem cell differentiation, chemotaxis, apoptosis, and metastasis. Here, we introduce Photonic Crystal Enhanced Microscopy (PCEM), and apply it to the study of murine dental stem cells to image the evolution of cell attachment and morphology during chemotaxis and drug-induced apoptosis. PCEM provides rich, dynamic information about the evolution of cell–surface attachment profiles over biologically relevant time-scales. Critically, this method retains the ability to monitor cell behavior with spatial resolution sufficient for observing both attachment footprints of filopodial extensions and intracellular attachment strength gradients.

Received 18th June 2013
Accepted 19th August 2013

DOI: 10.1039/c3an01541f

www.rsc.org/analyst

Introduction

Cell membrane interactions with surfaces are fundamental aspects of many *in vivo* biological phenomena including differentiation, growth, apoptosis, tumor metastasis and injury response.[1,2] Characterizing these processes in the laboratory traditionally involves fluorescent dyes, fluorescent proteins, histological stains, or fixation. Such approaches are either cytotoxic, or temporally constrained by the effects of fluorescence photobleaching. While these techniques elucidate the mechanics and outcomes of cellular processes, the lack of long-term, time-course data collection poses a serious compromise to the study of natural cell behavior during processes that occur over extended time scales like cell invasion[3] and chemotaxis.[4]

In order to address the challenges inherent in label-based cell imaging techniques, label-free microscopy technologies have been demonstrated as effective tools for measuring an increasingly diverse range of cellular processes.[5–8] Label-free microscopy involves a biosensor transducer surface that generates an electrical or optical signal when cells interact with it. Biosensors measure intrinsic cellular properties (such as dielectric permittivity) that can be used to determine the number of cells in contact with the transducer, or to determine the distribution of focal adhesion points. Such transducers may be prepared with surface coatings that either selectively capture specific cell populations through interaction with proteins expressed on their outer membranes or mimic the *in vivo* microenvironment within tissues.

Due to the fundamental importance of cell–surface interactions, several technologies have sought to quantify and image cell membrane adhesion. Surface Plasmon Resonance imaging (SPRi)[9] is capable of detecting cell attachment to a gold surface by measuring changes in the intensity of front-reflected light at a fixed angle and wavelength, but practical limitations degrade image quality. SPRi requires illumination to pass through cell structures, which introduces changes in reflected light intensity that are not related to cell surface attachment, and the lateral propagation distance of surface plasmons limits spatial resolution.[10] Interpretation of SPRi images is complicated by the variability of reflected light intensity introduced by scattering, inhomogeneity of the light source, and nonuniformity of the sensor surface,[11] while non-normal light *via* prism coupling hinders the quality of focus.[12] Atomic force microscopy (AFM)[13] has been used to study surface morphology and mechanical

[a]*Department of Electrical and Computer Engineering, Micro and Nanotechnology Laboratory, University of Illinois at Urbana-Champaign, 208 North Wright Street, Urbana, IL, 61801, USA. E-mail: bcunning@illinois.edu*

[b]*Department of Bioengineering, University of Illinois at Urbana-Champaign, Urbana, IL, USA*

[c]*Department of Chemical and Biomolecular Engineering, University of Illinois at Urbana-Champaign, Urbana, IL, USA*

[d]*Institute for Genomic Biology, University of Illinois at Urbana-Champaign, Urbana, IL, USA*

† Electronic supplementary information (ESI) available. See DOI: 10.1039/c3an01541f

‡ Co-authors who contributed equally to this work, listed alphabetically.

properties of cells by using a probe tip to collect localized force response. While it provides information about biological surfaces by making measurements from above, AFM does not analyse the interaction between cells and their substrates. In addition, as a probe scanning approach, the throughput of AFM is limited, enabling the study of only a small number of cells at once.

In this report, we demonstrate photonic crystal enhanced microscopy (PCEM) as a label-free biosensor-based cell attachment imaging approach that quantifies cell–surface interactions with spatial resolution sufficient for monitoring intra-cell attachment distribution, and temporal resolution sufficient for generating time-lapse movies during processes that include chemotaxis, apoptosis, differentiation, and division. Critically, these studies can be performed on extracellular matrix (ECM) protein functionalized substrates, retaining the capacity to define the chemistry of cell–matrix interactions. The system is integrated with an incubator, enabling long-term monitoring of cell attachment over substantial time scales (hours to days) without interruption of the culture environment. The key innovation enabling these capabilities is the use of noncoherent illumination of a photonic crystal biosensor and a spectroscopic scanning system that couples with a microscope objective. Here, we demonstrate label-free time-lapse imaging of the attachment and chemotaxis of dental stem cells using PCEM. Single-cell movement and filopodial extension are easily identifiable, yielding significant potential for the future investigation of numerous cellular processes including tumor cell metastasis and stem cell differentiation. While still an *in vitro* environment, the elimination of cytotoxic fluorophores and reporter molecules allows for the controlled study of complex biological processes over extended time periods.

Results

Photonic crystal biosensor surface engineered specifically for cell attachment

Photonic Crystal (PC) biosensors have recently been demonstrated as a highly versatile technology for a variety of label-free assays including high-throughput screening of small molecule–protein interactions, characterization of protein–protein interactions, and measurement of cell attachment modulation by drugs.[14–16] A PC is a sub-wavelength grating structure consisting of a periodic arrangement of a low refractive index material coated with a high reflective index layer (Fig. 1). When the PC is illuminated with a broadband light source, high order diffraction modes couple light into and out of the high index layer, destructively interfering with the zeroth-order transmitted light.[17] At a particular resonant wavelength and incident angle, complete interference occurs and no light is transmitted, resulting in 100% reflection efficiency. The resonant wavelength is modulated by the addition of biomaterial upon the PC surface, resulting in a shift to a higher wavelength. The electromagnetic standing wave that is generated at the PC surface during resonant light coupling inhibits lateral propagation, thus enabling neighboring regions on the PC surface to display a distinct resonant wavelength that is determined only by the density of biomaterial attached at that precise location. By measuring the resonant peak wavelength value (PWV) on a pixel-by-pixel basis over a PC surface, an image of cell attachment density may be recorded. PWV images of the PC may be gathered by illuminating the structure with collimated white light through the transparent substrate, while the front surface of the PC is immersed in aqueous media.

The advantages of PC-based surfaces for cell attachment imaging are compelling. As a label-free technology, cell attachment to a PC sensor is measured without the use of dyes or stains, so a population of cells can be measured repeatedly without disrupting their culture environment. The detected output signal is highly quantitative, providing measurements that are repeatable between sensors, instruments, and laboratories without photobleaching. PC biosensors are fabricated from inexpensive materials and require only low intensity illumination from beneath the sensor, so no electrical or physical contact between the sensor and the detection system occurs, and illumination does not pass through the cell body, the cell media, or the liquid–air meniscus of a microplate well. The PC biosensor strictly limits lateral propagation of resonantly coupled light, enabling imaging-based detection with resolution sufficient for measuring subtle variations in cell adhesion strength within a single cell, without needing to pre-tune the sensor to a particular resonant coupling condition, as in SPRi. PC biosensor imaging provides information that is fundamentally different than that provided by an optical microscope, as the sensor responds to local variation in cell attachment strength to the transducer surface. The sensor can be prepared with a variety of surface functionalizations (such as matrix coatings, antibodies, and peptides) and thus can be used as a tool for measuring how cell attachment to surfaces is modulated by drugs, growth factors, or other environmental factors.

Hyperspectral imaging microscope detection instrument

A schematic diagram of the PCEM instrument is shown in Fig. 2. The system is built upon the body of a standard microscope (Carl Zeiss Axio Observer Z1), but in addition to ordinary bright field imaging, a second illumination path is provided from a fiber-coupled broadband LED (Thorlabs M617F1, $600 < \lambda < 650$ nm). The fiber output is collimated and filtered by a polarizing beamsplitter cube to illuminate the PC with light that is polarized with its electric field vector oriented perpendicular to the grating lines. The polarized beam is focused by a cylindrical lens ($f = 200$ mm) to form a linear beam at the back focal plane of the objective lens (10×, Zeiss). After passing through the objective lens, the orientation of the line-shaped beam is rotated to illuminate the PC from below at normal incidence. The reflected light is projected, *via* a side port of the inverted microscope and a zoom lens, onto a narrow slit aperture at the input of an imaging spectrometer. The width of the adjustable slit was set to 30 μm for the work reported here. Using this method, reflected light is collected from a linear region of the PC surface, where the width of the imaged line, 1.2 μm, is determined by the width of the entrance slit of the imaging spectrometer and the magnification power of the objective lens. The system

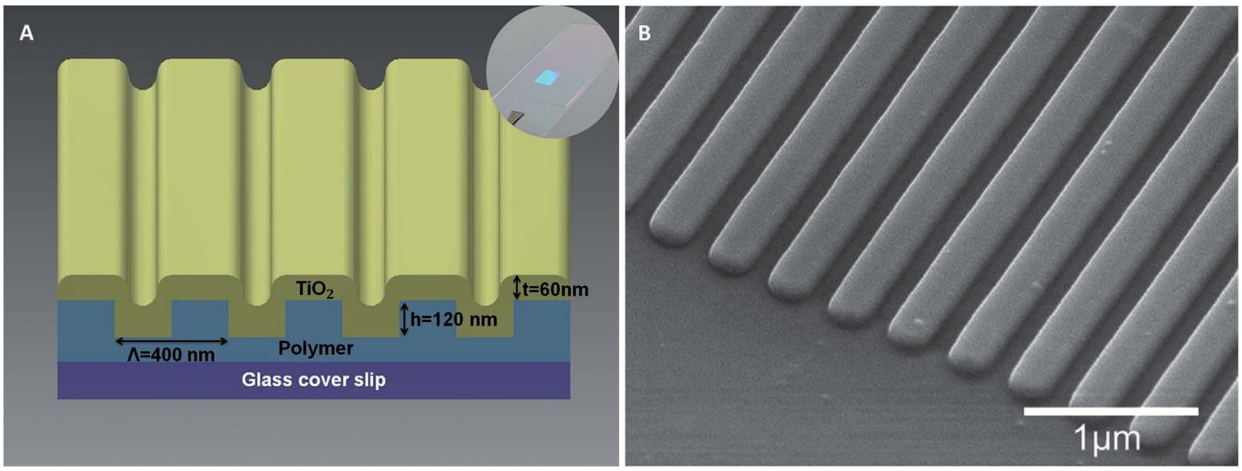

Fig. 1 (A) Schematic diagram of the photonic crystal (PC) biosensor. A PC sensor is comprised of a replica molded polymer grating overcoated with a high refractive index thin film of TiO_2. Inset: photo of a PC fabricated upon a glass cover slip. (B) Scanning electron micrograph of the PC surface.

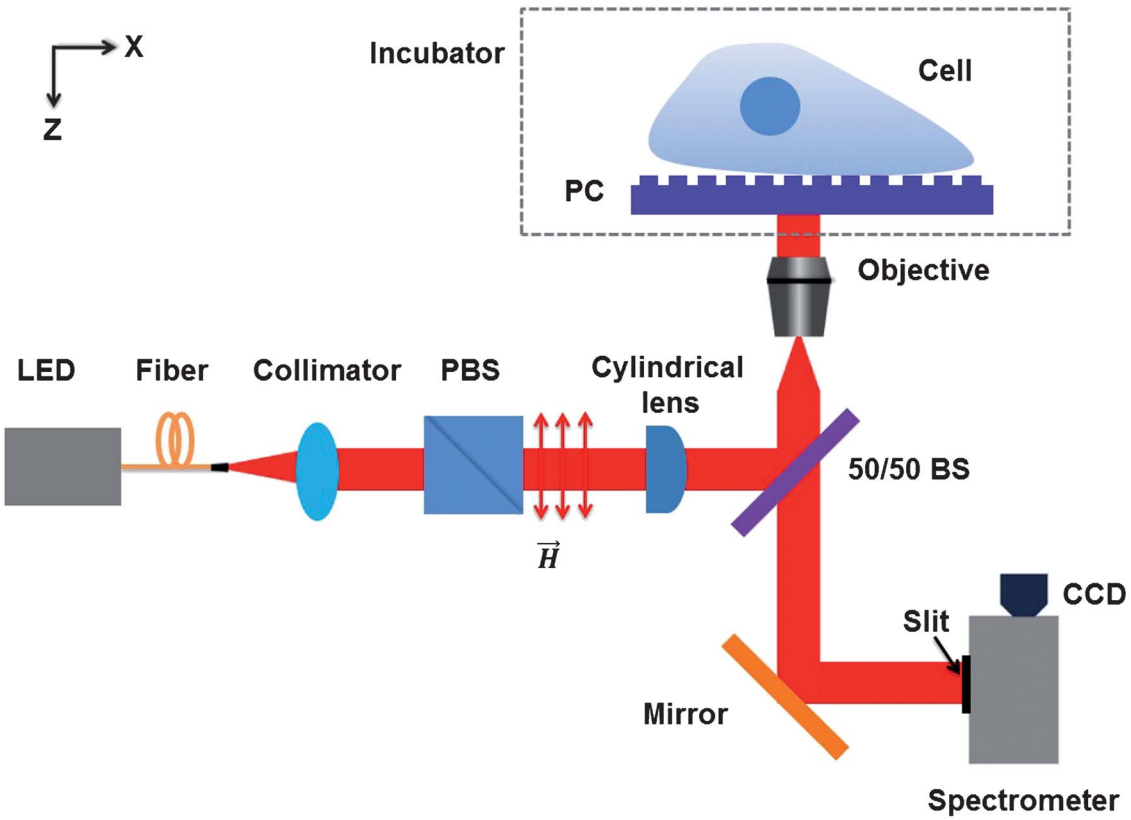

Fig. 2 Instrument schematic of the PCEM. Illumination from a fiber-coupled LED is collimated and passed through a polarizing beamsplitter (PBS) to create a pure electric field polarization perpendicular to the PC grating. A cylindrical lens focusses the light to a line at the back focal plane of the objective. The PC resonantly reflects only a narrow band of wavelengths, which are collected through the entrance slit of an imaging spectrometer.

incorporates a grating-based spectrometer (Acton Research) with a 512 × 512 pixel CCD camera (Photometrics Cascade 512). The line of reflected light, containing the resonant biosensor signal, is diffracted by the grating within the spectrometer (300 lines per mm) to produce a spatially resolved spectrum for each point along the line.

Therefore, each pixel across the line is converted to a resonant reflection spectrum, containing a narrow bandwidth ($\Delta\lambda \sim$ 4 nm) reflectance peak from the PC. The Peak Wavelength Value (PWV) of each peak is determined by fitting the spectrum to a 2nd order polynomial function, and then mathematically determining the maximum wavelength of the function. By

fitting all 512 spectra, in a process that takes 20 ms, a line comprised of 512 pixels is generated that represents one line of a PWV image of the PC surface. With an effective magnification of 26×, each pixel in the line represents a ~0.6 μm region of the PC surface and 512 such pixels cover a total width of ~300 μm. To generate a two-dimensional PWV image of the PC surface, a motorized stage (Applied Scientific Instruments, MS2000) translates the sensor along the axis perpendicular to the imaged line in increments of 0.6 μm per step. Using this technique, a series of lines are assembled into an image at a rate of 0.1 s per line and the same area on the PC surface can be scanned repeatedly. Each image is comprised of 512 by n pixels, where n can be selected during each scan session, and each pixel represents a 0.6 × 0.6 μm region of the PC surface. A biosensor experiment involves measuring shifts in PWV. A baseline PWV image is gathered before the introduction of cells, when the PC is uniformly covered by cell media, which is aligned and mathematically subtracted from subsequent PWV images gathered during and after cell attachment.

Characterization of the PC sensitivity and resonant wavelength stability under cell culture conditions

In preparation for cell attachment demonstrations, the ability of the PCEM to measure shifts in the bulk refractive index of the cell media was established. First, exposing the entire PC surface to distilled water ($n = 1.333$) and subsequently exposing the same sensor to isopropyl alcohol ($n = 1.377$), we confirmed that an individual pixel within a PCEM image demonstrates high reflection efficiency and narrow resonant reflection bandwidth (ESI, Fig. S1†). The PWV shift measured from a single pixel exposed to both media yielded a bulk refractive index sensitivity of $\Delta\lambda/\Delta n = 102$ nm/RIU.

A series of PWV images were gathered over a 12 hour period to demonstrate PWV stability with the PC exposed to cell media at the elevated temperature ($T = 37$ °C) and 5% CO_2 environment used for biological studies. Ham's F12 media (Invitrogen) was placed in a PDMS well attached to the PC surface. The average PWV shifted by only 0.12 nm over 12 hours, and the standard deviation of PWV within an image of a PC uniformly exposed to cell media was 0.09 nm (ESI, Fig. S2†).

Label free imaging of intracellular attachment and morphological changes

The most commonly used method for identification of differentiating stem cells is the labor- and time-intensive methylcellulose assay, which only reveals the identity of the colonies weeks after commitment occurs.[18–20] Furthermore, this approach requires cells to be resuspended in liquid phase, thereby altering many of the environmental cues that yielded the observed differential development. Using PCEM, it is possible to capture the dynamics of cell morphology and cell–matrix interactions during complex processes such as stem cell differentiation under real-time conditions (with less than 60 seconds between subsequent images). Such a tool would be critical for examining the potential of cell attachment signatures as a proxy for stem cell lineage commitment, particularly considering such analyses could be performed without disturbing the extracellular environment.

As cells attach and spread, positive PWV shifts are observed due to an increase in the concentration of cellular material within the evanescent field region of the PC. A PWV image for human pancreatic cancer cells (Panc-1) is compared to a brightfield image of the same cells in Fig. 3. Morphological profiles are consistent with healthy, attachment-dependent cells. Representative spectra are shown from inside and outside the cell region, demonstrating a definitive whole-spectrum shift of the characteristic resonant peak. Clearly visible boundaries of ~0.5 nm PWV shifts demonstrate the ability of PCEM to provide information about the geometry of attachment, which has been shown to have significant implications for both the classification of differentiating stem cells,[21] and the metastatic potential of tumor cells.[22] In addition, sub-cellular variation of PWV is indicative not only of the presence of cellular adhesion, but also modulation in the strength of attachment. For example, cell '2' in Fig. 3 shows a gradient in cell attachment strength from left to right. A region of greater PWV shift along the leading edge suggests the formation of lamellipodia, indicating a higher concentration of intracellular matter than is present in the rest of the cellular attachment footprint. As it can be assumed that the majority of this lower-PWV shifted footprint occurs under regions of cytosol, the increased PWV of the cell boundary, especially in these protrusions, most likely can be attributed to the formation of actin bundles at sites of focal adhesion, a process thoroughly documented *via* traditional, yet cytotoxic, fluorescent staining techniques.[23–25]

Label free imaging of stem cell attachment and drug-induced apoptosis

Next, murine dental stem cells (mHAT9a) were cultured and allowed to attach to a PC surface prepared with fibronectin over a period of two hours (Fig. 4a, ESI, Video S1†). From the series of PWV images gathered at 3 minute intervals, initial attachment times can be identified within the 3 minute period of image acquisition. Cells are observed attaching to the treated surface, with initial attachment characterized by small, round areas of PWV shift, consistent with spherical cells exiting suspension. As time progresses, average cell diameter increases, and membrane boundaries become more irregular as cellular processes begin to extend from cell bodies. Many cells maintain highest shifts at their periphery, which is consistent with the high concentration of cytoskeletal protein necessary for boundary maintenance and lamellar extension.[26] Random locomotion is observable, which reveals that cellular detachment results in a full recovery of initial PWV values when a cell moves to a new location. We observe no preference for the cells to extend themselves or to move along the direction of the PC grating.

Cellular apoptosis and detachment were also studied. Using another fibronectin-treated PC biosensor, mHAT9a cells were allowed to attach to the sensor surface for 3 hours. A final concentration of 2 μM staurosporine, shown to induce apoptosis *via* protein kinase inhibition,[27,28] was added to the cell chamber and mixed for 15 seconds. Cells were imaged every

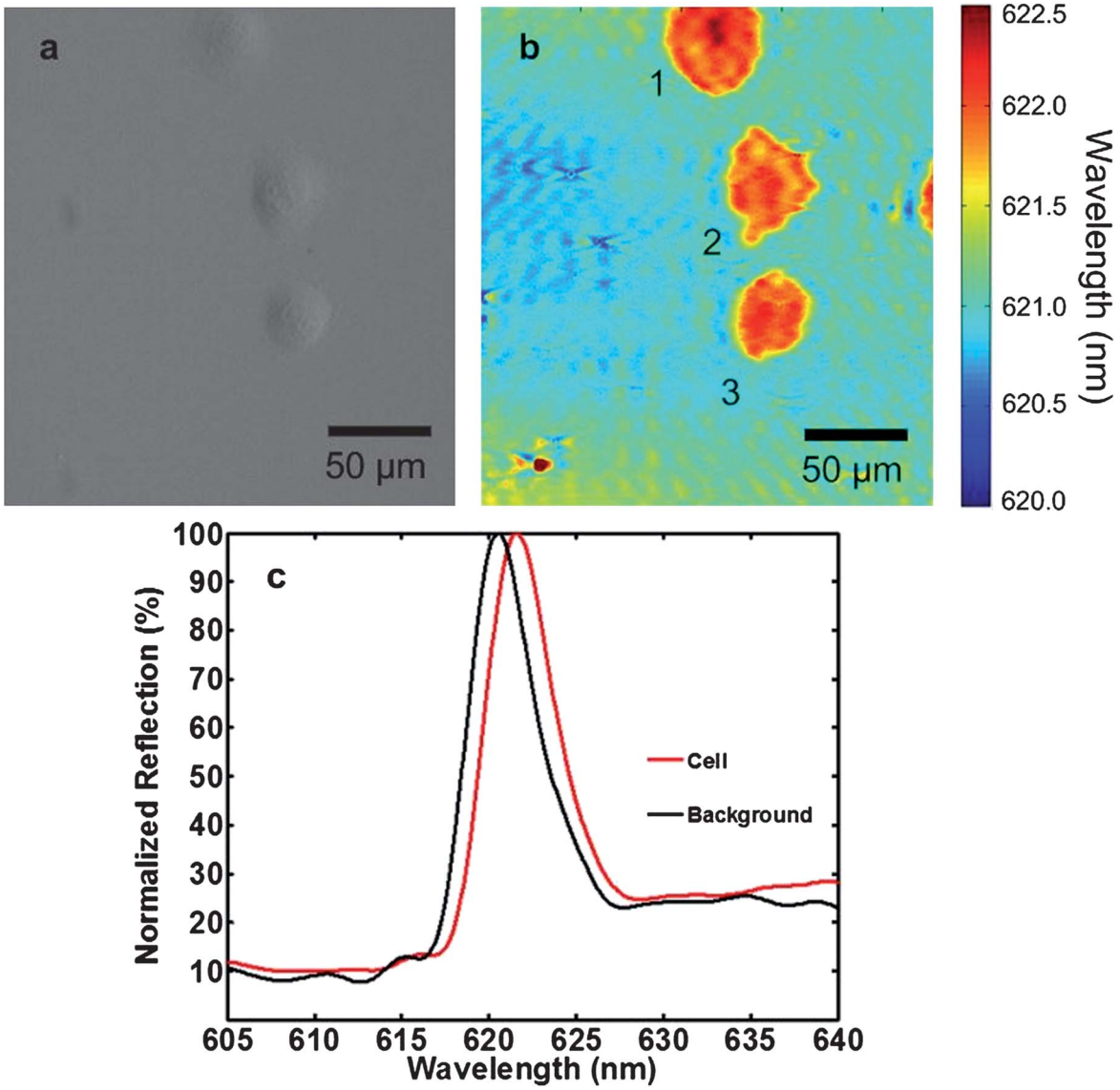

Fig. 3 (a) Bright field and (b) PWV imaging of Panc-1 cells attached to the PC surface. Cells were seeded onto a fibronectin-coated sensor and allowed to incubate for 2 hours before imaging. Lamellipodial extensions are visible, especially from cell 2, demonstrating the ability of PCEM to resolve regional differences in single-cell attachment. Darker shading indicates regions of higher protein concentration, and is present in regions near the boundary of lamellipodia formation, consistent with the creation of actin bundles. (c) Representative regions of cellular attachment. Selected areas of the PWV image from beneath a cell show the PWV shift of a typical Panc-1 cell is ~1.0 nm, and consistent throughout the entire spectrum at those locations.

20 minutes for 18 hours (Fig. 4b, ESI, Video S2†). Initial cells appear healthy, with various filopodia extending radially from cell bodies. As time progresses, the footprint of the cell bodies decreases, and several of the cells appear to detach completely. Other cells appear to undergo apoptosis prior to detachment, leaving behind remnants of cell membrane, which still produce a detectable PWV shift. The breakdown and modification of cell–cell and cell–ECM interactions is of great importance to answering questions about the progression of cancer cell detachment and metastasis from primary tumor sites. PCEM is unique in the fact that the biosensor response is a direct quantification and 2D localization of attachment at the single cell level, as opposed to indirect methods of staining for actin bundle formation or even ensemble averaging of bulk dielectric properties. This direct observation available over a time scale of hours to days provides a natural tool for the future study of cancer cell detachment and metastasis.

Label free imaging of stem cell chemotaxis

We next sought to validate the use of PCEM imaging in examining cell-mediated chemotaxis. The importance of stromal cell-derived factor-1 (SDF-1α) in the directed chemotaxis of differentiating cells is well-known for a myriad of situations including hypoxic ocular neovascularization, capillary formation and adipocyte differentiation in human adipose tissue, and bone regeneration in traumatic brain injury.[29–31] More recently, SDF-1α and its effect in attracting CXCR4 receptor positive cells have

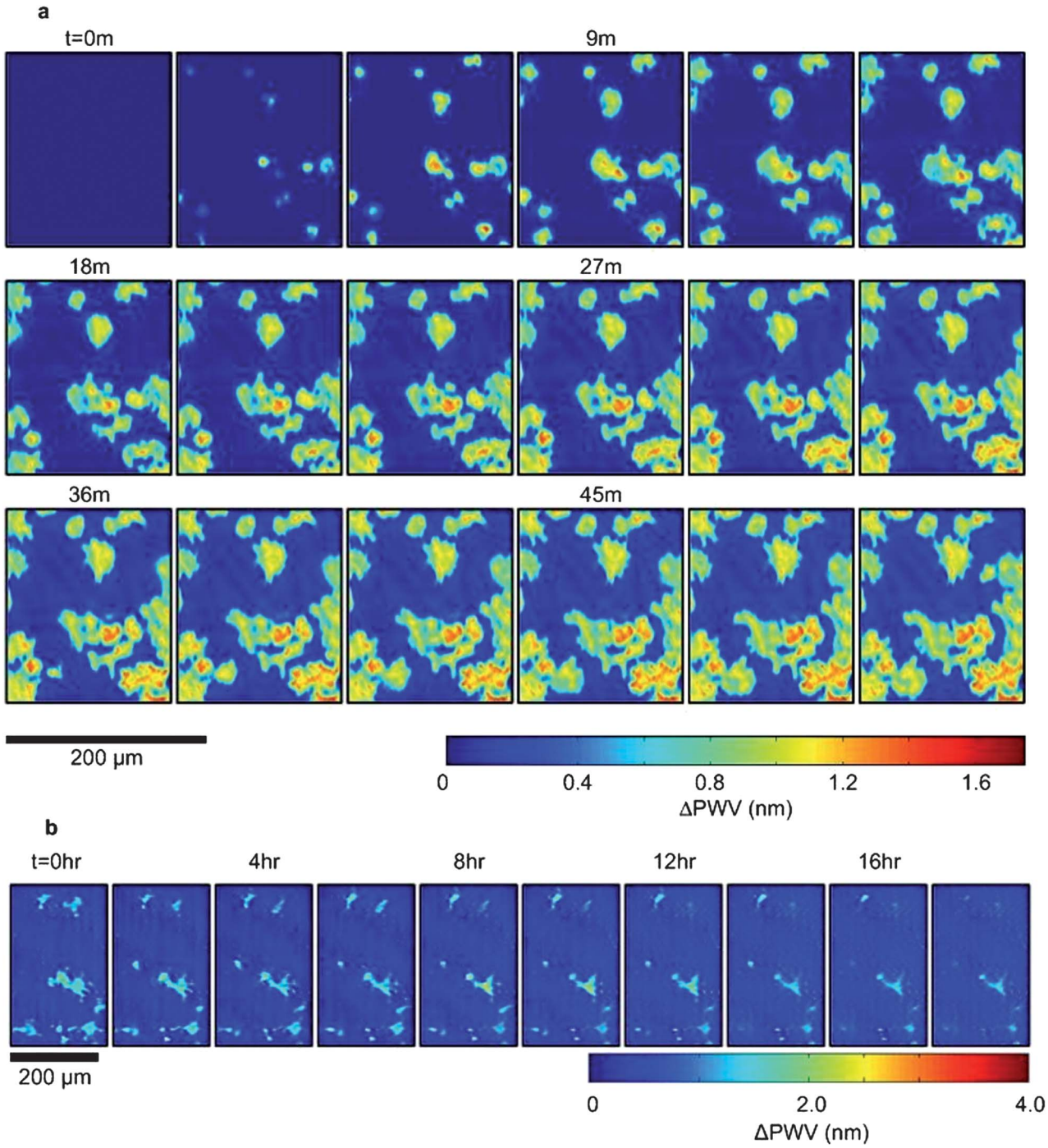

Fig. 4 (a) Time lapse PWV images of cellular attachment of mHAT9a cells. Cells were seeded at 20 000 cells per ml on a fibronectin-coated sensor surface. After 3 minutes, regions initial cell attachment appear as small, round regions, consistent with spheroid, trypsinized cells coming out of suspension and attaching to a surface. As time progresses, both the size of the cells and intensity of the PWV shift induced by them increases, indicating a higher localization of cellular material at the sensor surface, which can be expected during cell spreading. Finally, once cells are sufficiently attached, cellular processes can be observed sensing the cells' microenvironment in all directions. The outer irregular boundaries of the cells have a relatively low PWV, consistent with thin, exploratory filopodia, accompanied by a more heavily attached region slightly immediately adjacent in the cell interior, likely a result of actin bundle formation. (b) Time lapse PWV images of mHAT9a apoptosis and detachment. Cells were seeded at 8000 cells per ml onto a fibronectin-coated sensor surface. Cells that detach can be observed by the gradual retraction of filopodia and overall cell rounding before the PWV shift disappears entirely. Some cells appear to undergo apoptosis while still attached, leaving remnants of cell membranes and protein on the sensor surface. ΔPWV data was attained *via* background subtraction from an initial image taken before cell attachment ($t = 0$). For movies, see ESI, Videos S1 and S2.†

been investigated in dental healing and regeneration. However, current mechanisms for studying the recruitment of dental stem cells have been based on fixing and staining cells.[32,33] As the observed migration occurs on the order of days, label-based assays are not feasible for extended time course studies. PCEM provides an opportunity to monitor such events as they occur.

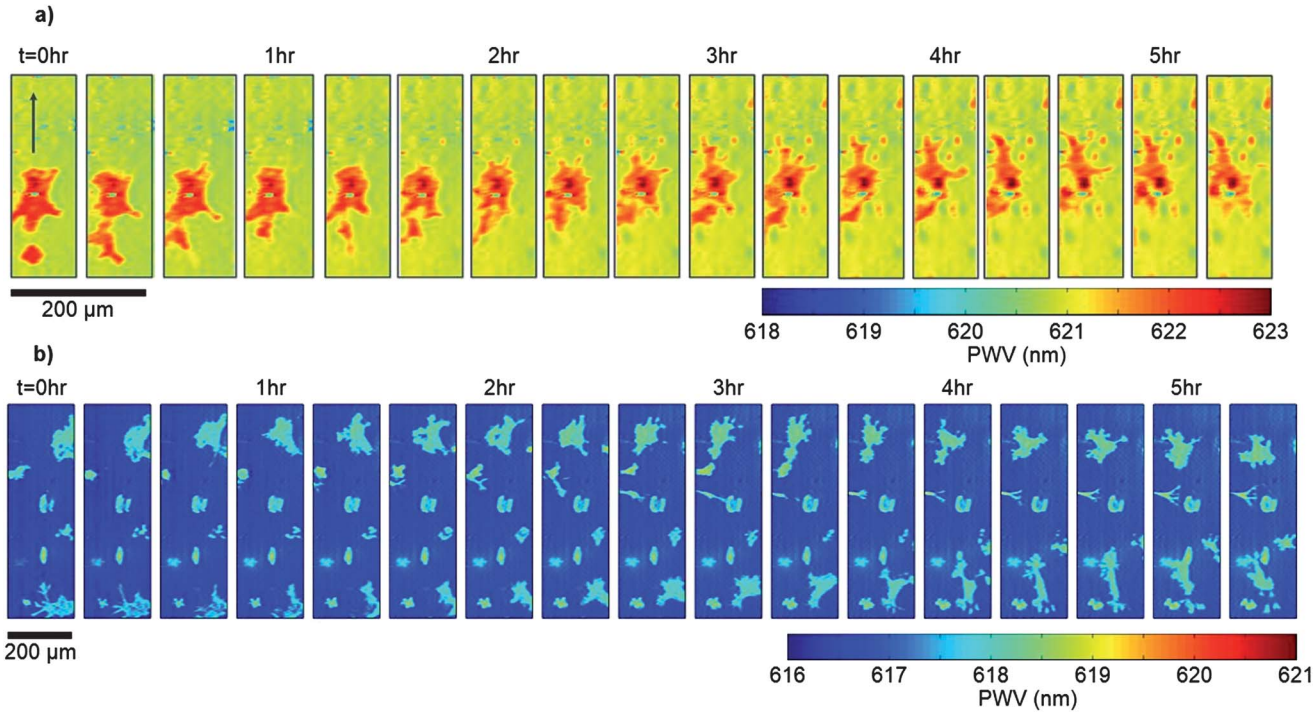

Fig. 5 (a) Time lapse PWV images of chemotaxis of mHAT9a cells. Cells were deposited on the sensor surface at a concentration of 8000 cells per ml and allowed to attach for 2 hours before imaging. An agarose bead was placed at a location approximately 100 microns above the top of the image, and PWV images were collected every 20 minutes after the bead was placed. Cell movement direction is indicated with an arrow in the leftmost frame. (b) CXCR4 knockout cells exhibit non-directional movement on the sensor surface. Similarly prepared, CXCR4 mutants do not show directional movement toward the bead, demonstrating that the previously observed directional locomotion was due to chemotaxis. For movies, see ESI, Videos S3 and S4.†

We examined mHAT9a chemotaxis in response to beads soaked in SDF-1α, a chemoattractant to which the receptor CXCR4 is sensitive[34] (Fig. 5, ESI, Videos S3 and S4†). After a bead was placed on the sensor surface, attached cells were observed to move in the direction of the eluting bead. Probing lamellipodia extend in multiple directions around the cell, but only projections formed in the direction of the bead are maintained by the migrating cells. Attachment in the trailing edge of the cell decreases over time as the cell bodies proceed in the direction of chemotaxis, resulting in a return of the sensor to its native state. The experiment was repeated with a mHAT cell line with a constitutive knockout of the CXCR4 coding gene, and no directional movement was observed. This suggests that the observed cellular movement was indeed due to chemotaxis, as opposed to nonspecific locomotion. Critically, we do not observe preferential movement or extension of cell processes in the direction of the PC grating lines. To our knowledge, this represents the first label-free time-lapse imaging of the attachment localization of living cells during chemotaxis.

It has been shown that SDF-1α/CXCR4 mediated recruitment of dental stem cells is likely an important inflammatory response and underlying promoter of reparative dentin formation.[35] Further investigation of the SDF-1α/CXCR4 pathway with the PCEM technology could provide a valuable investigation of morphological changes induced by the inflammatory response of dental stem cells to dental damage.

Conclusions

PCEM represents a new imaging modality that can be easily integrated with a conventional optical microscope to enable quantified, near real-time, high resolution imaging of cell–surface interactions. While traditional microscopy techniques such as phase-contrast and DIC provide basic information about cellular morphology and general appearance, PCEM provides information that is specific to the interface between the cell and its substrate. By virtue of the surface-confined resonant electric field of the photonic crystal, PCEM enables high contrast imaging of the interaction strength of cells with a surface, providing a specific attachment footprint as opposed to a generalized shape of the entire three-dimensional cell body. The approach utilizes low power illumination from a visible wavelength LED from below, using a PC sensor structure that can be incorporated into standard coverslips (as demonstrated here), microscope slides, or microtiter plates that are typically used for cell research. PCEM clearly demonstrates that cell–surface attachment strength is not uniformly distributed within a cell or static as a function of time, but instead contains rich dynamic information that includes the rate of cell boundary extension, the size of a cell "footprint" on a surface, and the effect of the extracellular environment (including chemotactic gradients) on cell attachment.

The cell imaging experiments used to demonstrate PCEM were selected to show that the spatial resolution of the approach

is sufficient for clearly observing features such as spatial gradients in cell–surface attachment and the extension of fine-structured filopodia, attributes that are typically observed only using dyes or stains. As a label-free detection approach, PCEM enables continuous monitoring of these phenomena over extended time periods that are compatible with the biological time scales of chemotaxis, apoptosis, differentiation, and proliferation. This work demonstrates, to our knowledge, the first time-lapse movies of cell–surface interaction monitoring at these time scales (ESI, Videos S1–S4†).

It is already well-established that both the comparison of cancerous/non-cancerous cells and of cell lineages differentiated from pluripotent stem cells lend themselves to investigation *via* their unique morphologies and cellular attachment protein expression, with the majority of such differences easily visible *via* traditional microscopy. With PCEM, cellular attachment morphology can be directly observed, and attachment 'profiles' for different cell types can be developed. By limiting the study of cell morphology to the specific density of cellular material present in the evanescent field region of a photonic crystal, attachment can be observed in a more direct method with less subjectivity than simple qualitative observation using traditional microscopy methods.

There is an increasing awareness of the importance of cellular adhesion and the mechanical microenvironment of cells on their behavior, yet directly measuring these attributes in a non-invasive fashion has proved difficult. PCEM provides a novel, robust methodology for the investigation of these attributes in a controlled environment without chemical alteration. The relationship between mechanical microenvironmental cues and cancer cell behavior has been demonstrated, contributing significantly to tissue dysplasia and metastatic detachment.[36] With PCEM, it will be possible to investigate important components within the progression of tumor-development, such as the recruitment and movement of neutrophils to the cancer microenvironment. Neutrophil polarization and chemotaxis represents a challenging process to study as it presents a complex and dynamic set of cellular–ECM interactions. Near real-time imaging would allow for rapid improvement in our understanding of this and the other biological applications discussed herein, providing dynamic attachment information that is not currently available.

Materials and methods

Nanoreplica molding of PC sensors

The PC sensors used in this study were fabricated using a low-cost nanoreplica molding manufacturing approach that has been described previously.[37] Briefly, a silicon wafer molding template with a negative volume image of the desired PC grating structure (period = 400 nm, depth = 120 nm) was fabricated using deep-UV lithography and reactive ion etching. Liquid UV-curable epoxy was pressed between a glass cover slip (0.17 mm thick) and the silicon wafer, and was subsequently cured to a solid using a high intensity UV lamp. The hardened epoxy preferentially adhered to the glass substrate and was peeled away from the silicon wafer, leaving a replica of the silicon mold. A thin TiO_2 layer ($t \sim 60$ nm) was deposited *via* reactive RF sputtering (PVD 75, Kurt Lesker) providing the high-refractive index coating. Fig. 1B presents a scanning electron micrograph of the replica-molded sensor after dielectric coating and shows excellent uniformity across the PC surface. The final grating height is ~80 nm, as measured by atomic force microscope, to provide a surface that does not contain deep or abrupt grooves that may influence cellular attachment processes. The PC is designed to resonantly reflect a wavelength of $\lambda \sim 620$ nm, with $\Delta\lambda = 4$ nm attributed to aqueous immersion (ESI, Fig. S1†).

Cell culture

Murine dental stem cells (mHAT9a) were attained from the Harada Lab.[38] Stable cultures of both the wild type and CXCR4 deficient mutant were maintained in Dulbecco's Modified Eagle Medium supplemented with B-27 serum free supplement (Invitrogen), 20 ng ml^{-1} bFGF and 20 ng ml^{-1} EGF (Peprotech). Deficient mutant cells were not cultured more than fourteen days before use due to passage number-associated mutations. Panc-1 pancreatic carcinoma cells (ATCC) were maintained in DMEM supplemented with 10% FBS and 4 mM L-glutamine.

Sensor preparation

PCs were sonicated for one minute in acetone, followed by cleaning with IPA and water. After thorough drying with N_2, devices were oxygen-plasma treated for 5 minutes to facilitate attachment of a liquid containment gasket. A polydimethylsiloxane (PDMS) gasket with an internal area of 1.2×1.2 mm^2 was prepared with a thickness of 8 mm. After application of the gasket well, the PC surface was hydrated with PBS, and a layer of fibronectin was adsorbed to promote cellular attachment. The sensor was inserted into a custom holder attached to the motorized stage of the microscope, followed by PWV image scanning.

Chemotaxis investigation

mHAT9a cells were attached to a fibronectin-treated PC biosensor. Two hours after attachment, soaked beads were warmed to 37 °C and placed in the PCEM field of view using the eyepiece of the microscope for targeting. PCEM images were acquired at 20 minute intervals for a total duration of 10 hours.

Acknowledgements

We are thankful for the support provided by the U.S. Army Medical Research & Materiel Command (USARMC) *via* the Telemedicine & Advanced Technology Research Center (TATRC) under Contract no. W81XWH0810701. Additionally, we would like to thank the National Science Foundation (NSF) for their support under CBET 11-32301 and Grant no. 1254738. Any opinions, findings, conclusions, or recommendations expressed in this material are those of the authors and do not necessarily reflect the views of the NSF. This work was also partially supported by Grant #189782 from the American Cancer Society of Illinois. The authors are also grateful for additional funding provided by the Department of Chemical & Biomolecular Engineering and the Institute for Genomic Biology at the University of Illinois at

Urbana-Champaign. mHAT cells were a gift of Dr Hidemitsu Harada (Iwate Medical University, Japan) and we acknowledge Dr Tamaki Yokohama-Tamaki (Health Sciences University of Hokkaido, Japan) for assistance with mHAT cell culture.

References

1 J. Boudreau and P. L. Jones, *Biochem. J.*, 1999, **339**, 481–488.
2 M. Barczyk, S. Carracedo and D. Gullberg, *Cell Tissue Res.*, 2010, **339**, 269–280.
3 T. L. Frandsen, B. E. Boysen, S. Jirus, J. Zwiebel, M. Spangthomsen, E. W. Thompson and N. Brunner, *Fibrinolysis*, 1992, **6**, 71–76.
4 W. J. Rosoff, J. S. Urbach, M. A. Esrick, R. G. McAllister, L. J. Richards and G. J. Goodhill, *Nat. Neurosci.*, 2004, **7**, 785–785.
5 M. M. A. Jamil, M. C. T. Denyer, M. Youseffi, S. T. Britland, S. Liu, C. W. See, M. G. Somekh and J. Zhang, *J. Struct. Biol.*, 2008, **164**, 75–80.
6 A. W. Peterson, M. Halter, A. Tona, K. Bhadriraju and A. L. Plant, *BMC Cell Biol.*, 2009, **10**, 1–17.
7 B. Lin, P. Y. Li and B. T. Cunningham, *Sens. Actuators, B*, 2006, **114**, 559–561.
8 R. McGuinness, *Curr. Opin. Pharmacol.*, 2007, **7**, 535–540.
9 B. Rothenhausler and W. Knoll, *Nature*, 1988, **332**, 615–617.
10 M. E. Caldwell and E. M. Yeatman, *Appl. Opt.*, 1992, **31**, 3880–3891.
11 F. Bardin, A. Bellemain, G. Roger and M. Canva, *Biosens. Bioelectron.*, 2009, **24**, 2100–2105.
12 T. M. Chinowsky, T. Mactutis, E. Fu and P. Yager, *Proc. SPIE*, 2004, **5261**, 173–182.
13 G. Binnig, C. F. Quate and C. Gerber, *Phys. Rev. Lett.*, 1986, **56**, 930–933.
14 B. Cunningham, P. Li, B. Lin and J. Pepper, *Sens. Actuators, B*, 2002, **81**, 316–328.
15 B. T. Cunningham, P. Li, S. Schulz, B. Lin, C. Baird, J. Gerstenmaier, C. Genick, F. Wang, E. Fine and L. Laing, *J. Biomol. Screening*, 2004, **9**, 481–490.
16 P. C. Mathias, S. I. Jones, H. Y. Wu, F. Yang, N. Ganesh, D. O. Gonzalez, G. Bollero, L. O. Vodkin and B. T. Cunningham, *Anal. Chem.*, 2010, **82**, 6854–6861.
17 D. Rosenblatt, A. Sharon and A. A. Friesem, *IEEE J. Quantum Electron.*, 1997, **33**, 2038–2059.
18 M. Winkler, N. Trieu, T. Feng, L. Jin, S. Walker, L. Singh and H. T. Ku, *J. Visualized Exp.*, 2011, e3148.
19 N. I. zur Nieden, J. T. Cormier, D. E. Rancourt and M. S. Kallos, *J. Biotechnol.*, 2007, **129**, 421–432.
20 C. L. Miller and B. Lai, in *Basic Cell Culture Protocols*, Springer, 2005, pp. 71–89.
21 C. Seiler, A. Gazdhar, M. Reyes, L. M. Benneker, T. Geiser, K. A. Siebenrock and B. Gantenbein-Ritter, *J. Tissue Eng. Regener. Med.*, 2012, DOI: 10.1002/term.1575.
22 X. Tang, Q. Wen, T. B. Kuhlenschmidt, M. S. Kuhlenschmidt, P. A. Janmey and T. A. Saif, *PLoS One*, 2012, **7**, e50443.
23 B. Wehrle-Haller and B. A. Imhof, *Int. J. Biochem. Cell Biol.*, 2003, **35**, 39–50.
24 G. Cooper, in *The Cell: A Molecular Approach*, ed. G. Cooper, Sunderland, MA, 2004, ch. 11.
25 J. T. Smith, J. T. Elkin and W. M. Reichert, *Exp. Cell Res.*, 2006, **312**, 2424–2432.
26 M. Nemethova, S. Auinger and J. V. Small, *J. Cell Biol.*, 2008, **180**, 1233–1244.
27 B. S. Cummings, G. R. Kinsey, L. J. C. Bolchoz and R. G. Schnellmann, *J. Pharmacol. Exp. Ther.*, 2004, **310**, 126–134.
28 M. W. Karaman, S. Herrgard, D. K. Treiber, P. Gallant, C. E. Atteridge, B. T. Campbell, K. W. Chan, P. Ciceri, M. I. Davis, P. T. Edeen, R. Faraoni, M. Floyd, J. P. Hunt, D. J. Lockhart, Z. V. Milanov, M. J. Morrison, G. Pallares, H. K. Patel, S. Pritchard, L. M. Wodicka and P. P. Zarrinkar, *Nat. Biotechnol.*, 2008, **26**, 127–132.
29 C. Sengenès, A. Miranville, M. Maumus, S. de Barros, R. Busse and A. Bouloumié, *Stem Cells*, 2007, **25**, 2269–2276.
30 R. L. e Silva, J. Shen, S. F. Hackett, S. Kachi, H. Akiyama, K. Kiuchi, K. Yokoi, M. C. Hatara, T. Lauer and S. Aslam, *FASEB J.*, 2007, **21**, 3219–3230.
31 X. Liu, C. Zhou, Y. Li, Y. Ji, G. Xu, X. Wang and J. Yan, *PLoS One*, 2013, **8**, e54077.
32 L. Jiang, Y.-Q. Zhu, R. Du, Y.-X. Gu, L. Xia, F. Qin and H. H. Ritchie, *J. Endod.*, 2008, **34**, 939–944.
33 T. Suzuki, C. Lee, M. Chen, W. Zhao, S. Fu, J. Qi, G. Chotkowski, S. Eisig, A. Wong and J. Mao, *J. Dent. Res.*, 2011, **90**, 1013–1018.
34 M. Kucia, K. Jankowski, R. Reca, M. Wysoczynski, L. Bandura, D. J. Allendorf, J. Zhang, J. Ratajczak and M. Z. Ratajczak, *J. Mol. Histol.*, 2004, **35**, 233–245.
35 Q. M. Gong, J. J. Quan, H. W. Jiang and J. Q. Ling, *J. Endod.*, 2010, **36**, 1499–1503.
36 S. Kumar and V. M. Weaver, *Cancer Metastasis Rev.*, 2009, **28**, 113–127.
37 B. Cunningham, B. Lin, J. Qiu, P. Li, J. Pepper and B. Hugh, *Sens. Actuators, B*, 2002, **85**, 219–226.
38 K. Otsu, R. Kishigami, N. Fujiwara, K. Ishizeki and H. Harada, *J. Cell. Physiol.*, 2011, **226**, 2527–2534.

